Hindawi
Journal of Electrical and Computer Engineering
Volume 2019, Article ID 2609235, 14 pages
https://doi.org/10.1155/2019/2609235

Research Article

Implementation of Static Line Voltage Stability Indices for Improved Static Voltage Stability Margin

Natakorn Thasnas and Apirat Siritaratiwat

Department of Electrical Engineering, Khon Kaen University, Khon Kaen 40002, Thailand

Correspondence should be addressed to Apirat Siritaratiwat; apirat@kku.ac.th

Received 10 December 2018; Revised 8 March 2019; Accepted 27 March 2019; Published 2 May 2019

Academic Editor: Salvatore Favuzza

Nowadays, the changes of economic, environment, and regulations are forcing the electric utilities to operate systems at maximum capacity. Therefore, the operation and control of power system to improve the system stability has been receiving a great deal of attention. This paper presents an approach for enhancing the static voltage stability margin and reducing the power losses of the system with voltage security-constrained optimal power flow (VSC-OPF) that is based on static line voltage stability indices. The control approaches incorporate the voltage stability criteria into the conventional OPF. The minimization of the summation of fast voltage stability index (FVSI), line stability index (L_{mn}), and line voltage stability index (LVSI) is used as the objective functions. The performance and effectiveness of the proposed control approaches are evaluated on the standard IEEE 30-bus, 57-bus, and 118-bus test systems under normal and contingency conditions. The comparison analysis is carried out with different cases including minimization of generation cost. The proposed control approaches indicate the promising results and offer efficient countermeasures against the voltage instability of the system.

1. Introduction

Voltage instability is recognized as the major sources of power system insecurity, for which several partial or full power interruptions have been related to this problem. Nowadays, electric power systems have been operating closer to their stability limit. Hence, this problem is a great challenge for power system stability and control [1–5]. The main factor causing instability is the inability of the power system to transfer reactive power to load, which can be avoided by enhancing the static voltage stability margin. One effective approach is to control the system parameters by formulating the voltage stability issue into the conventional optimal power flow (OPF) problem. Thus, there is renewed interest to develop the voltage security-constrained optimal power flow (VSC-OPF) approach, ensuring the system is operating at a secure level [4–8].

In the literature, the voltage stability criterion is incorporated into the OPF formulation with different approaches. These can be classified into two categories, i.e., voltage stability objective function and constraint. For the objective function to improve stability margin, several studies have introduced bus voltage indices into the OPF problem, which has been an efficient method for enhancing the voltage stability. One example is the objective function to minimize the sum of the squares of L-index, which can provide the optimal setting of various control devices against voltage collapse [8]. The modified objective function based on the L-index enhances the voltage stability margin for normal and contingency conditions in some research studies [9–13]. The minimal eigenvalue of the nonsingular Jacobian matrix improves the voltage stability [14, 15]. The system loadability was formulated into a multiobjective optimization technique; the problem formulation is to minimize the generation cost and maximize the voltage security margin [16, 17]. Other voltage stability indicators have been proposed to approximate the distance to voltage collapse, and these were incorporated into the objective function [18–20].

With respect to incorporation of the voltage stability constraint, many other studies have reported that it can

control the system in a secure manner. The reactive reserve-based contingency constrained optimal power flow (RCCOPF) concept was formulated as the reactive reserve constraint to improve the voltage stability margin of post-contingency states [21]. The L-index was adapted as the voltage stability constraint to maintain the voltage level in an economical way [22, 23]. The voltage security-constrained OPF (VSC-OPF) formulation that incorporates margin enhancement constraints (MEC) was proposed in [24] to control the reactive power for the given voltage stability criteria. The minimum load increase for system instability was considered in terms of the voltage stability margin (VSM), which was used as the constraint for the OPF problem when rescheduling the generation and adjusting the contact transactions for an independent system operator (ISO) [25]. Load impedance modulus margin (LIMM) was employed for the first time for VSC-OPF as a complementary voltage stability constraint [26]. A minimum singular value (MSV) was developed into VSC-OPF model based on semidefinite programming (SDP) relaxation [27]. The incorporation of line voltage collapse index (VCI) was proposed for line-wise optimal power flow as the set of voltage stability constraint and objective function [28].

Few studies have used the line voltage stability indices in the OPF problem. The VSC-OPF approach based on the voltage collapse proximity indicator (VCPI) has been presented and included in OPF formulation in two ways, the proposed objective function and constraint [29]. The fast voltage stability index (FVSI) was proposed as an objective function to identify the best location of an unified power flow controller (UPFC) with the goal of enhancing the voltage profile and minimizing system losses [30]. The line stability index (LQP) was incorporated in the OPF formulation as an objective function for finding the optimal location of the static synchronous series compensator (SSSC) and static VAR compensator (SVC) [31]. Line voltage stability index (LVSI), operating cost, and emission effects were proposed as the objective function of stochastic optimal power flow problem with the presence of uncertain wind power generations [32]. Five voltage stability indices (VSIs), i.e., L-index, fast voltage stability index (FVSI), line stability index (L_{mn}), online voltage stability index (LVSI), and voltage collapse proximity indicator (VCPI), were employed in VSC-OPF to compare their performances [33].

As previously mentioned, incorporation of the static line voltage stability indices into the OPF problem has not extensively been investigated. Moreover, these indices provide accurate information about the proximity to voltage collapse. Both voltage variation and power are incorporated into the indices [29]. For this reason, the strong performance of the static line voltage stability indices motivated the authors of this study to investigate the voltage security-constrained optimal power flow (VSC-OPF) based on static line voltage stability indices.

This study is focused on incorporating the static line voltage stability indices into the conventional OPF formulation to improve the static voltage stability margin and power losses of the system. The fast voltage stability index (FVSI), line stability index (L_{mn}) and line voltage stability index (LVSI) are used for the proposed approaches. The OPF objective functions are based on the minimization of the total sum of the indices. The performance and effectiveness of the proposed control approaches are investigated under both normal and contingency conditions, and they are compared with different cases, including minimization of generation cost. Furthermore, this paper is organized as follows. Section 2 provides a description of the FVSI, L_{mn}, and LVSI indices. The OPF problem formulation with consideration of the voltage stability is given in Section 3. The OPF computational algorithm is described in Section 4. Section 5 explains the implementation of the proposed algorithm. In Section 6, interesting results are presented and interpreted. Finally, major contributions and conclusions are stated in Section 7.

2. Static Line Voltage Stability Indices

Static line voltage stability indices are formulated based on the power transmission concept of a two-bus system. A single line of the two-bus system is illustrated in Figure 1. These indices incorporate the voltage stability index for each line connection between two bus bars. P_r is the real power at the receiving end. Q_r is the reactive power at the receiving end. V_s and V_r are the voltages at the sending and receiving ends. δ_s and δ_r are the phase angles at the sending and receiving buses. Z is the line impedance. R is the line resistance. X is the line reactance. θ is the line impedance angle.

2.1. Fast Voltage Stability Index (FVSI). Musirin [34] proposed the fast voltage stability index (FVSI). This index is formulated from the voltage quadratic equation of the two-bus system, as shown in Figure 1. FVSI is based on the concept of power flow through the line of the network and defined as follows:

$$\mathrm{FVSI} = \frac{4Z^2 Q_r}{V_s^2 X}. \tag{1}$$

An FVSI less than 1.00 indicates a stable condition. If the FVSI is close to 1.00, the particular line is close to instability. If the FVSI goes beyond 1.00, the bus voltage will suddenly drop, resulting in system collapse.

2.2. Line Stability Index (L_{mn}). The line stability index (L_{mn}) was proposed by Moghavvemi [35]. It is derived from a concept that is similar to the FVSI as presented in Figure 1. The value of the L_{mn} index can be calculated as follows:

$$L_{mn} = \frac{4XQ_r}{\left[V_s \sin(\theta - \delta)\right]^2}. \tag{2}$$

It is defined $\delta = \delta_s - \delta_r$. To identify the voltage stability of each line, the interpretation is similar to the FVSI. The line is close an unstable condition when the L_{mn} index is close to 1.00. If the value is greater than 1.00, the system will experience voltage collapse.

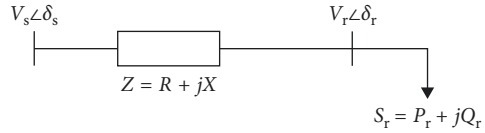

Figure 1: Two-bus system.

2.3. Line Voltage Stability Index (LVSI). Naishan et al. [36] formulated the line voltage stability index (LVSI). This index is similar to the L_{mn} index, but it is derived from the relationship between the reactive power at the receiving end and voltage at the sending end. The LVSI formulation is given as follows:

$$\text{LVSI} = \frac{4RP_r}{\left[V_s \cos(\theta - \delta)\right]^2}. \tag{3}$$

The LVSI is used to identify the system conditions that are similar to the FVSI and L_{mn} index as previously mentioned.

All static line voltage stability indices use a combination of system variables and elements of the admittance matrix, which is simple and requires less computation. In addition, the limits of the system elements, such as the VAR limits of the generators, can be considered in the analysis. Therefore, these indices are flexible to simulate any type of load pattern and system network. One disadvantage of such indices is the limitation in the estimation accuracy. They only express the critical lines. However, based on equations (1) to (3), if the total sum of the indices is formulated as the objective function of the OPF problem, the lower index values result in the better enhancement of voltage stability margin.

3. Problem Formulation

The optimal power flow (OPF) aims to identify the optimal solution for an objective function that is subject to several equality and inequality constraints, such as the power flow constraints, system operating limit constraints, and limits on equipment. The general OPF formulations are determined as follows [37]:

$$\begin{aligned} &\text{minimize} && f(x, u), \\ &\text{subject to} && g(x, u) = 0, \\ &&& h(x, u) \le 0, \end{aligned} \tag{4}$$

where f represents the objective function, g is the equality constraints, and h is the inequality constraints. x is a vector of state variables including slack bus active power, load bus voltages, generator reactive powers, and apparent power flows, which is expressed as follows:

$$x = \left[P_{\text{gslack}},\ V_{\text{d1}}, \ldots, V_{\text{d}N_{\text{d}}},\ Q_{\text{g1}}, \ldots, Q_{\text{g}N_{\text{g}}},\ S_{\text{l1}}, \ldots, S_{\text{l}N_{\text{l}}}\right], \tag{5}$$

where P_{gslack} is the active power generation at slack bus, $V_{\text{d}i}$ is the load voltage at bus i. N_{d} is the number of load buses, $Q_{\text{g}i}$ is the reactive power generation at bus i, N_{g} is the number of total generators, $S_{\text{l}i}$ is the apparent power flow at branch i, and N_{l} is the number of transmission lines.

u is a vector of control variables consisting of active power generations except at slack bus, generator bus voltages, transformer tap ratios, and reactive powers of shunt compensation capacitors, expressed as

$$u = \left[P_{\text{g}i}, \ldots, P_{\text{g}N_{\text{g}}},\ V_{\text{g1}}, \ldots, V_{\text{g}N_{\text{g}}},\ T_1, \ldots, T_{N_{\text{tran}}},\ Q_{\text{c1}}, \ldots, Q_{\text{c}N_{\text{cap}}}\right], \tag{6}$$

where $P_{\text{g}i}$ is the active power generation at bus i, $V_{\text{g}i}$ is the generator bus voltage at bus i, T_i is the transformer tap ratio at bus i, N_{tran} is the number of transformer taps, Q_{ci} is the shunt compensation capacitor at bus i, and N_{cap} is the number of compensation capacitors.

3.1. Objective Function

3.1.1. Minimization of the Total Fuel Cost for Active Power Generation. This objective function aims to minimize the total fuel cost of active power injection. It is a simple summation of the individual polynomial cost functions of active power generation for each generator. And the power generation is the control variable for this function. It is defined as follows:

$$f_c(x) = \sum_{i=1}^{n_g}\left(a_i + b_i P_{g_i} + c_i P_{g_i}^2\right), \tag{7}$$

where $f_c(x)$ is the total fuel cost, n_g is the number of generator buses; a_i, b_i, and c_i are the ith generator cost coefficients; and P_{g_i} is the real power injection of the ith generator.

3.1.2. Voltage Stability Improvement Based on the Minimization of the Summation of the Static Line Voltage Stability Indices. The static line voltage stability indices are incorporated into the conventional OPF problem as the objective functions. The purpose of objective functions is to minimize the summation of stability indices. The control variables involve active power generation except at slack bus and generator bus voltages. Three objective functions are proposed as follows:

(i) Voltage stability margin enhancement based on the FVSI:

$$f_{\text{FVSI}}(x) = \sum_{i=1}^{n_l} \text{FVSI}_i, \tag{8}$$

where $f_{\text{FVSI}}(x)$ is the total sum of the FVSI. n_l is the number of transmission lines of the system. FVSI_i is the value of the FVSI for the ith transmission line.

(ii) Voltage stability margin enhancement based on L_{mn}:

$$f_{L_{mn}}(x) = \sum_{i=1}^{n_l} L_{mn_i}, \tag{9}$$

where $f_{L_{mn}}(x)$ is the total sum of L_{mn}. n_l is the number of transmission lines of the system. L_{mn_i} is the value of L_{mn} for the ith transmission line.

(iii) Voltage stability margin enhancement based on the LVSI:

$$f_{\mathrm{LVSI}}(x) = \sum_{i=1}^{n_{\mathrm{l}}} \mathrm{LVSI}_i, \tag{10}$$

where $f_{\mathrm{LVSI}}(x)$ is the total sum of the LVSI. n_{l} is the number of transmission lines of the system. The LVSI_i is the value of the LVSI for the ith transmission line.

3.2. System Constraints. There are three types of constraints of the OPF problem worth considering. Equations (11) to (20) describe all system constraints [37].

3.2.1. Equality Constraints. These equality constraints are the set of the real and reactive power balance equations:

$$P_{\mathrm{g}_i} - P_{\mathrm{d}_i} = V_i \sum_{j=1}^{N} V_j \left(G_{ij}\cos\theta_{ij} + B_{ij}\sin\theta_{ij}\right), \quad i = 1, \ldots, N, \tag{11}$$

$$Q_{\mathrm{g}_i} - Q_{\mathrm{d}_i} = V_i \sum_{j=1}^{N} V_j \left(G_{ij}\sin\theta_{ij} + B_{ij}\cos\theta_{ij}\right), \quad i = 1, \ldots, N, \tag{12}$$

where P_{g_i} and Q_{g_i} are the real and reactive power injections of the ith generator. P_{d_i} and Q_{d_i} are the real and reactive power loads at bus i. V_i and V_j are the voltage magnitude at buses i and j. G_{ij} and B_{ij} are the transfer conductance and susceptance between buses i and j, respectively. θ_{ij} is the phase angle difference between buses i and j. N is the total number of system buses.

3.2.2. Inequality Constraints.

$$P_{\mathrm{g}_i}^{\min} \le P_{\mathrm{g}_i} \le P_{\mathrm{g}_i}^{\max}, \quad i = 1, \ldots, N_{\mathrm{g}}, \tag{13}$$

$$Q_{\mathrm{g}_i}^{\min} \le Q_{\mathrm{g}_i} \le Q_{\mathrm{g}_i}^{\max}, \quad i = 1, \ldots, N_{\mathrm{g}}, \tag{14}$$

$$V_{\mathrm{g}_i}^{\min} \le V_{\mathrm{g}_i} \le V_{\mathrm{g}_i}^{\max}, \quad i = 1, \ldots, N_{\mathrm{g}}, \tag{15}$$

$$\left|S_{\mathrm{L}_i}\right| \le S_{\mathrm{L}_i}^{\max}, \tag{16}$$

$$V_{\mathrm{d}_i}^{\min} \le V_{\mathrm{d}_i} \le V_{\mathrm{d}_i}^{\max}, \quad i = 1, \ldots, N_{\mathrm{d}}, \tag{17}$$

$$Q_{\mathrm{c}_i}^{\min} \le Q_{\mathrm{c}_i} \le Q_{\mathrm{c}_i}^{\max}, \quad i = 1, \ldots, N_{\mathrm{cap}}, \tag{18}$$

$$T_i^{\min} \le T_i \le T_i^{\max}, \quad i = 1, \ldots, N_{\mathrm{tran}}, \tag{19}$$

where $P_{\mathrm{g}_i}^{\min}$ and $P_{\mathrm{g}_i}^{\max}$ are the minimum and maximum active power generations at bus i. $Q_{\mathrm{g}_i}^{\min}$ and $Q_{\mathrm{g}_i}^{\max}$ are the minimum and maximum reactive power generations at bus i. $V_{\mathrm{g}_i}^{\min}$ and $V_{\mathrm{g}_i}^{\max}$ are the minimum and maximum generator voltages at bus i. S_{L_i} and $S_{\mathrm{L}_i}^{\max}$ are the apparent power flow and its maximum at branch i. $V_{d_i}^{\min}$ and $V_{d_i}^{\max}$ are the minimum and maximum load voltages at bus i. $Q_{\mathrm{c}_i}^{\min}$ and $Q_{\mathrm{c}_i}^{\max}$ are the minimum and maximum shunt compensation capacitances at bus i. $T_i^{\min}$ and $T_i^{\max}$ are the minimum and maximum transformer tap ratios at bus i.

3.2.3. Constraint Handling. The integration of inequality of dependent variables into the penalized objective function should be maintained within their limits to refuse infeasible solutions. These variables are including slack bus active power generation, load bus voltage magnitudes, reactive power generations, and apparent power flows. The penalty function can be expressed as follows [38]:

$$\begin{aligned} J(x,u) = {} & f(x,u) + K_P\left(P_{\mathrm{gslack}} - P_{\mathrm{gslack}}^{\lim}\right)^2 \\ & + K_V \sum_{i=1}^{N_{\mathrm{load}}} \left(V_{\mathrm{d}_i} - V_{\mathrm{d}_i}^{\lim}\right)^2 + K_Q \sum_{i=1}^{N_{\mathrm{line}}} \left(Q_{\mathrm{g}_i} - Q_{\mathrm{g}_i}^{\lim}\right)^2 \\ & + K_S \sum_{i=1}^{N_{\mathrm{line}}} \left(S_{\mathrm{L}_i} - S_{\mathrm{L}_i}^{\max}\right)^2, \end{aligned} \tag{20}$$

where $J(x,u)$ is the penalized objective function; K_p, K_Q, K_V, and K_s are the penalty factors; and $x^{\lim}$ is the limit value of the dependent variables, determined as follows:

$$x^{\lim} = \begin{cases} x^{\max}, & \text{if } x > x^{\max}, \\ x, & \text{if } x^{\min} < x < x^{\max}, \\ x^{\min}, & \text{if } x < x^{\min}. \end{cases} \tag{21}$$

4. Computational Algorithm

The computational procedure of the VSC-OPF problem is presented in the flowchart of Figure 2. The optimization algorithm of this study is a hybrid DA-PSO optimization algorithm. This hybrid algorithm was proposed by Khunkitti et al. [37]. It is the combination of the exploration phase of the dragonfly algorithm (DA) and exploitation phases of particle swarm optimization (PSO) algorithm. Its performance is superior to other optimization algorithms for finding the optimal solution of the OPF problem. Therefore, this study uses this technique to solve the VSC-OPF problem. The explanation of related optimization algorithms and hybrid DA-PSO optimization algorithm is as follows.

4.1. Dragonfly Algorithm (DA). The dragonfly algorithm is a metaheuristic algorithm. It was inspired by the static and dynamic swarming behaviors of dragonflies in nature [39]. The goals of swarming are hunting (static swarm) and migration (dynamic swarm). In the hunting, dragonflies move in larger swarms and along one direction, which is appropriated in the exploitation phase. In the dynamic swarm, when roaming over long distances and different

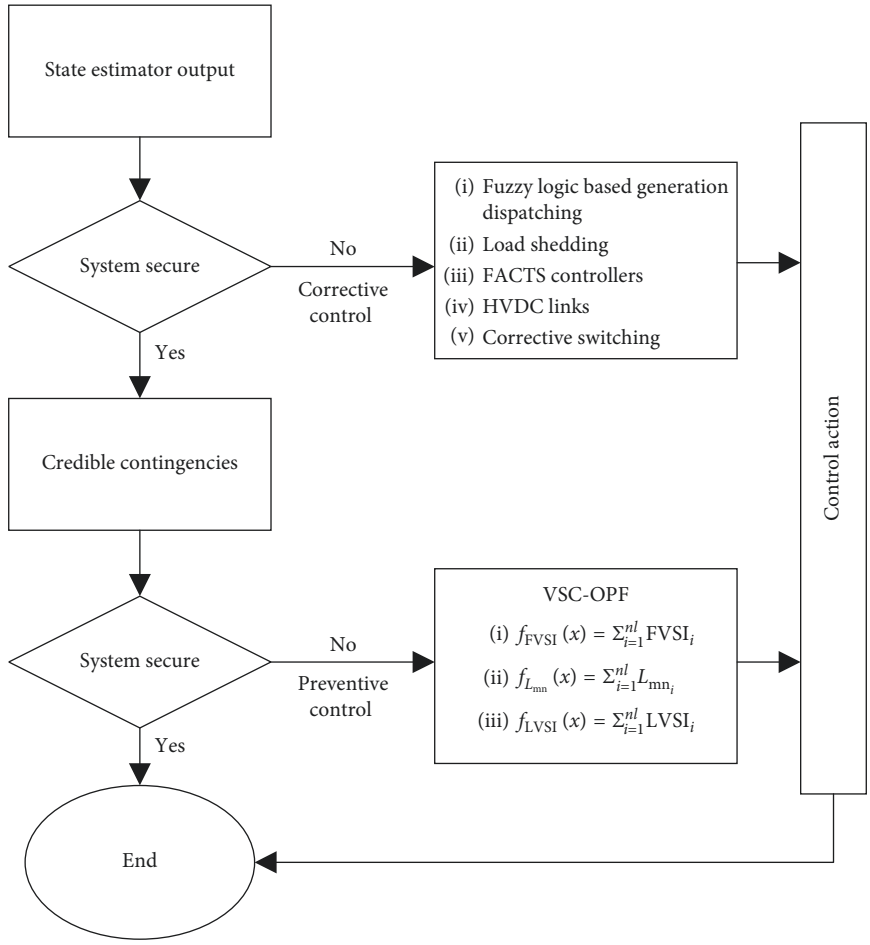

Figure 2: The schematic of a few functions performed in the energy control center (ECC).

areas, many dragonflies will swarm which is suitable in the exploration phase.

Separation, alignment, cohesion, attraction to a food source, and distraction of an enemy represent the behavior of dragonflies. The described and formulated of these behaviors are as follows:

(i) Separation: it is the avoidance of the static crashing of individuals into other individuals in the neighborhood, which is formulated in the following equation:

$$S_i = -\sum_{j=1}^{N} X - X_j, \tag{22}$$

where S_i is the separation of the ith individual. N is the number of neighboring individuals. X is the position of the current individual. X_j is the position of jth neighboring individual.

(ii) Alignment: it represents the velocity matching of individuals to the velocity of others in the neighborhood. It is able to compute by the following equation:

$$A_i = \frac{\sum_{j=1}^{N} V_j}{N}, \tag{23}$$

where A_i is the alignment of the ith individual and V_j is the velocity of the jth neighboring individual.

(iii) Cohesion: it is the proclivity of individuals to the center of mass of the neighborhood. It can be calculated by the following equation:

$$C_i = \frac{\sum_{j=1}^{N} X_j}{N} - X, \tag{24}$$

where C_i is the cohesion of the ith individual.

(iv) Attraction to a food source: it should be the main objective of any swarm to survive. And it is computed by the following equation:

$$F_i = X^+ - X, \tag{25}$$

where F_i is the food source of the ith individual and X^+ is the position of the food source.

(v) Distraction of an enemy: it is another survival objective of the swarm, which is formulated in the following equation:

$$E_i = X^- - X, \tag{26}$$

where E_i is the position of enemy of the ith individual and X^- is the position of the enemy source.

The movement of artificial dragonflies and updation of their positions are simulated by considering the step vector (ΔX) and position vector (X). The step vector demonstrates the direction of the movement of the artificial dragonflies, which is formulated in the following equation:

$$\Delta X^{t+1} = \left(sS_i + aA_i + cC_i + fF_i + eE_i\right) + \omega^t \Delta X^t, \quad (27)$$

where ΔX^{t+1} is the step vector at iteration $t+1$. ΔX^t is the step vector at iteration t; s, a, c, f, and e are the separation weight, alignment weight, cohesion weight, food factor, and enemy factor, respectively. ω^t is the inertia weight factor at iteration t and is calculated by the following equation:

$$\omega^t = \omega_{\max} - \frac{\omega_{\max} - \omega_{\min}}{\text{Iter}_{\max}} \times \text{Iter}, \quad (28)$$

where $\omega_{\max}$ and $\omega_{\min}$ are set to 0.9 and 0.4, respectively; Iter is the iteration; and $\text{Iter}_{\max}$ is the maximum iteration.

The position of the artificial dragonflies is able to be updated by the following equation:

$$X^{t+1} = X^t + \Delta X^{t+1}, \quad (29)$$

where X^{t+1} is the position at iteration $t+1$ and X^t is the position at iteration t.

In case the search space is not able to find a neighboring solution, stochastic behavior need to be improved by the moving of the artificial dragonflies around the search space with the application of random walk (Lévy flight). For this case, the position of the dragonflies can be calculated as follows:

$$X^{t+1} = X^t + \text{Lévy}\,(\text{d}) \times \text{X}^{\text{t}}, \quad (30)$$

where Lévy is the Lévy flight which is computed by the following equation and d is the dimension of the position vectors:

$$\text{Levy}\,(d) = 0.01 \times \frac{r_1 \times \sigma}{\left|r_2\right|^{1/\beta}}, \quad (31)$$

where r_1 and r_2 are the two uniform random values in a range of [0,1]. σ is calculated by the following equation:

$$\sigma = \left(\frac{\tau(1+\beta) \times \sin(\pi\beta/2)}{\tau(1+\beta/2) \times \beta \times 2^{(\beta-1/2)}}\right)^{1/\beta}, \quad (32)$$

where β is the constant. $\tau(x) = (x-1)!$.

4.2. Particle Swarm Optimization (PSO). Particle swarm optimization is a population-based stochastic global optimization technique which was first introduced in [40]. For this approach, each particle represents a possible solution with a movement of population around a multidimensional search space. The association of each particle and a fitness value can indicate the performance in the fitness space.

Each particle i consists of its position $X_i = (x_{i,1}, x_{i,2}, \ldots, x_{i,Nvar})$, where Nvar represents the number of control variables, velocity $V_i = (v_{i,1}, v_{i,2}, \ldots, v_{i,N\text{var}})$ and personal best experience $X_{\text{pbest}i} = (x_{\text{pbest}i,1}, x_{\text{pbest}i,2}, \ldots, x_{\text{pbest}i,N\text{var}})$, and a swarm has a global best experience $X_{\text{gbest}} = (x_{\text{gbest}1}, x_{\text{gbest}2}, \ldots, x_{\text{gbest,}N\text{var}})$. For each iteration, the direction of each particle will be own personal best position. However, the direction of the global best position can be obtained by particles in the swarm. The operation of each particle is expressed as follows:

$$V_i^{t+1} = \omega^t \times V_i^t + C_1 \times \text{rand}_1 \times \left(X^t_{\text{pbest}_i} - X_i^t\right) + C_2 \times \text{rand}_2 \times \left(X^t_{\text{gbest}} - X_i^t\right), \quad (33)$$

$$X_i^{t+1} = X_i^t + V_i^{t+1}, \quad (34)$$

where V_i^{t+1} is the velocity of particle i at iteration $t+1$. V_i^t is the velocity of particle i at iteration t. C_1 and C_2 are two positive acceleration constants. rand_1 and rand_2 are two uniform random values in a range of [0, 1]. $X^t_{\text{pbest}_i}$ is the personal best position of particle i at iteration t. X_i^t is the position of particle i at iteration t. X^t_{gbest} is the global best position among all particles at iteration t. X_i^{t+1} is the position of particle i at iteration $t+1$.

4.3. Hybrid DA-PSO Optimization Algorithm. The Hybrid DA-PSO algorithm combines the prominent points of the DA and PSO algorithms. At the beginning, the global solution is explored with the initialization of the dragonflies in DA. After obtaining the best position of DA, it will be substituted as the global best position in the PSO equation (equation (33)). Finally, in the exploitation phase, the PSO algorithm operates by using the global best position from DA, and the expected optimal solution can be obtained. To overcome this technique, the velocity and position equations of PSO should be modified as follows [37]:

$$V_i^{t+1} = \omega^t \times V_i^t + C_1 \times \text{rand}_1 \times \left(X^t_{\text{pbest}_i} - X_i^t\right) + C_2 \times \text{rand}_2 \times \left(X^t_{\text{gbest}} - X_i^t\right), \quad (35)$$

$$X_i^{t+1} = X_i^t + V_i^{t+1}, \quad (36)$$

where X^{t+1}_{DA} is the best position obtained from DA at iteration $t+1$.

The application of the DA-PSO algorithm for solving the OPF problem can be described as follows [37]:

Step 1. Initialize the system data including the parameters of DA and PSO, the number of dragonflies and particles, the number of iterations, and the archive size.

Step 2. Generate the initial population of dragonflies and particles.

Step 3. Convert the constrained multiobjective problem to an unconstrained one by using equation (20).

Step 4. Perform the power flow and calculate the objective functions for the initial population of dragonflies.

Step 5. Find the nondominated solutions and save them to the initial archive.

Step 6. Set the fitness value of the initial population as the food source.

Step 7. Calculate the parameters of DA (s, a, c, f, and e).

Step 8. Update the food source and enemy of DA.

Step 9. Evaluate the S, A, C, F, and E by using equations (22)–(26).

Step 10. Check if a dragonfly has at least one neighboring dragonfly, then update step vector (ΔX) and the position of dragonfly (X_{DA}) by equations (27) and (29), respectively, and if each dragonfly has no neighboring dragonfly, then update X_{DA} by using equation (30) and set ΔX to be zero.

Step 11. If any component of each population breaks its limit, then ΔX or X_{DA} of that population is moved into its minimum/maximum limit.

Step 12. Set the best position obtained from DA as the global best of PSO (X^{gbest}).

Step 13. Update the velocity of the particle (V) and the position of the particle (X_{PSO}) by using equations (35) and (36), respectively.

Step 14. If any component of each population breaks its limit, then V or X_{PSO} of that population is moved into its minimum/maximum limit.

Step 15. Calculate the objective functions of the new produced population.

Step 16. Employ the Pareto front method to save the nondominated solutions to the archive and update the archive.

Step 17. If the maximum number of iterations is reached, the algorithm is stopped; otherwise, go to Step 7.

5. Implementation of the Proposed Algorithm

The VSC-OPF algorithm is proposed in the previous section. This algorithm is incorporated into the energy control center (ECC) as the preventive control scheme [8]. Figure 2 shows the schematic of a few functions performed in ECC, which the online state estimator provides the outputs for system status. Network security analysis is categorized into two schemes, i.e., corrective control and preventive control schemes. For the corrective control scheme, the state estimator output is checked to verify the system stability. If the system is operating in nonsecure operating point, the corrective control scheme has to be taken. Then, different control actions can be applied to move the system into the secure level. Furthermore, after the contingency study, the preventive control scheme is performed when the system status is in the instability level. The proposed algorithm can be incorporated into ECC as the preventive control action for moving the operating point from the critical point and resulting in the adequate stability margin of the system.

6. Results and Discussion

This study is focused on incorporating the static line voltage stability indices into the conventional OPF formulation with the goal of enhancing static voltage stability margin and reducing power losses of the system. The IEEE 30-bus, 57-bus, and 118-bus test systems are used to assess and verify the performance and effectiveness of the proposed control approaches. The detailed data are as follows:

(i) The IEEE 30-bus test system includes six generators installed at buses 1, 2, 5, 8, 11, and 13. There are four transformers at lines 6–9, 6–10, 4–12, and 27–28 and 41 transmission lines. The total loads are 283.4 MW and 126.6 MVar. The network data are given in [41].

(ii) The IEEE 57-bus test system consists of seven generators located at buses 1, 2, 3, 6, 8, 9, and 12; 15 transformers; 80 transmission lines; and 42 loads totaling 1250.8 MW and 336.4 MVar, respectively. The detailed data are taken from [42].

(iii) The IEEE 118-bus test system has 54 generators, 9 transformers, and 186 transmission lines. The active and reactive power load demand of the system is 4242 MW and 1439 MVar, respectively. The complete data of these networks are given [43].

The results of this study are generated using a program developed in MATLAB [44]. The power flow and continuation power flow processes are accomplished with the help of MATPOWER [45]. The simulation results were generated to investigate the proposed control approaches for all the aforementioned test systems. Since the performance evaluation of the proposed VSC-OPF approach based on the line voltage stability indices is the main purpose of this study. Four different cases will be individually considered as part of the objective function in each system. The details of these cases are as follows:

(i) Case 1: the minimization of the generation cost is the objective function as shown in equation (6). The coefficients of generation cost are defined as in [33]. This study uses the results of this case as the base case to compare the performance with proposed approaches.

(ii) Case 2: the minimization of the total sum of FVSI in equation (8) is used as the objective functions. The lower the value of FVSI, the better the overall system voltage stability.

(iii) Case 3: the minimization of the total sum of L_{mn} in equation (9) is formulated as the objective functions of the OPF problem to enhance the voltage stability.

(iv) Case 4: the minimization of the total sum of LVSI in equation (10) is formulated as the objective functions similar to Cases 2 and 3.

6.1. System Performance. This section is to investigate the system performance of proposed approaches. For this study, the continuation power flow is used to determine the maximum loadability of the power system. The nose point of the P-V curve represents the maximum loadability; when the system reaches this point, any further increase in the active power transfer will lead to voltage collapse. The system

Table 1: System performance of the IEEE 30-bus test system.

	Objective functions			
	Case 1	Case 2	Case 3	Case 4
P_g (MW)	292.83	290.34	289.87	288.12
Q_g (MVar)	87.46	83.33	82.63	60.81
Loss (MW)	9.4290	6.9408	6.4713	4.7236
Cost ($/h)	802.21	829.11	831.09	971.55
Maximum FVSI	0.2471	0.0722	0.0672	0.4212
Maximum L_{mn}	0.2483	0.0723	0.0672	0.4221
Maximum LVSI	0.9019	0.8439	0.8631	0.7219
Sum FVSI	1.4519	0.6321	0.6273	2.4624
Sum L_{mn}	1.4694	0.6396	0.6349	2.4988
Sum LVSI	6.9357	6.6840	6.5508	5.2089
Maximum loadability (MW)	856.92	895.64	872.74	912.59

performance of the IEEE 30-bus test system is shown in Table 1. The comparisons of reactive power generation, transmission loss, and generation cost are indicated in Figure 3. It is clear that reactive power generation and transmission loss are significantly reduced with the objective functions of the minimization of the total sum of stability indices compared with the minimization of generation cost (Case 1). The reactive power generation of Case 1 is 87.46 MW, whereas Case 2, Case 3, and Case 4 perform better outcome with 83.33, 82.63, and 60.81 MVar, respectively. Case 4 is able to reduce 49.90% of loss compared with Case 1. Cases 2 and 3 also reduce the loss to 26.39% and 31.37%, respectively.

The maximum and summation values of stability indices of Cases 2, 3, and 4 are also improved from Case 1. These results follow the maximum loadability of the system. Case 4 provides the highest improvement in terms of the maximum loadability, which was 6.50% higher than Case 1. The maximum loadability values of Cases 2 and 3 are also increased from 856.92 MW (base case) to 895.64 MW and 872.74 MW, respectively. Total power generations are similar for all cases to meet the demand. All the proposed cases cost more than the base case. The total cost is increased from the base case by 3.35% for Case 2, 3.60% for Case 2, and 21.11% for Case 3. From the results, it can be observed that the proposed approach to incorporate LVSI index into objective function provides the best results because of its reduction of real power generation and loss, and its increase of system maximum loadability. But the high cost is the drawback of this case. The increment of fuel cost is imposed for the security cost.

The system performance of the IEEE 57-bus test system is indicated in Table 2, and Figure 4 shows the variable comparisons. The generation of real power is decreased from the base case by 17.93% for Case 2, 17.24% for Case 3, and 13.52% for Case 4. All the proposed cases also reduce the transmission loss with 14.77%, 20.15%, and 18.50% lower than the base cases for Case 2, Case 3, and Case 4, respectively. Moreover, Cases 2, 3, and 4 cost 0.70%, 0.60%, and 5.32% higher than the base cases, respectively. The maximum and summation values of FVSI, L_{mn}, and LVSI for all the proposed cases are improved. Maximum loadability of the system is enhanced from 2,395.84 MW for the base case to 2,441.80 MW for Case 2; 2,416.11 MW for Case 3; and 2,444.43 MW for Case 4. According to the results of the IEEE 57-bus test system, the minimization of L_{mn} case gives the best performance in terms of real power generation, loss, and cost. But the maximum loadability is highest in case of incorporation of LVSI.

The variable comparisons of the system performance for the IEEE 118-bus test system are shown in Table 3 and Figure 5. It is clear that the performance obtained in Cases 2, 3, and 4 is better than Case 1. The reactive power generation (Q_g) of Case 2 is 167.77 MVar less by 32.89% compared with base case while the Q_g values of Cases 3 and 4 are 232.22 MVar and 183.09 MVar. The highest reduction of transmission loss is provided by Case 2, a reduction of about 13.17%. Cases 3 and 4 are able to decrease the loss to 5.21% and 4.01%, respectively. All the proposed cases are higher the cost of generation by 3.77% for Case 2, 7.45% for Case 3, and 3.60% for Case 4 compared with Case 1. Finally, incorporating the line voltage stability indices can give voltage stability margin due to the improvement of the maximum and summation values of indices, and the computed results are shown in Table 3. The loadability is also enhanced to more secure level with the increment of 10.45% for Case 2 and 5.06% for Case 3 compared with Case 1, but Case 3 can give only 1.11% increase. It is obvious that the incorporation of FVSI into objective function produces the best result for the IEEE 118-bus test system.

6.2. PV Curves at the Weakest Bus. The PV curves at the weakest bus are also used to verify the effectiveness of the proposed control approach. The weakest bus is identified using the tangent vector. The analyzed tool for this section is similar to that in the previous section. The continuation power flow is employed to obtain the PV curves and tangent vector. Based on the simulation results, bus number 30 is the weakest bus of the IEEE 30-bus test system. The PV curves at the weakest bus for all case studies are shown in Figure 6. In the base case, the voltage collapses when the total load at bus number 30 reaches 1.3491 p.u. All proposed cases can improve the static voltage stability margin of the system. Case 4 gives the highest total load at 1.4801 p.u. (9.71% enhancement). Cases 2 and 3 are able to increase the total load to 1.4402 p.u. (6.75% enhancement) and 1.3863 p.u. (2.76% enhancement).

The PV curves at the weakest bus of the IEEE 57-bus test system are shown in Figure 7. Bus number 37 is the weakest bus. Total load of Case 1 (base case) is 0.6103 p.u., that is, lower than 4.01% compared with Case 2 (0.6348 p.u.). Case 3 also raises margin to 0.6211 p.u. Case 4 can increase the highest margin with 4.24% enhancement (4.24 p.u.).

Bus number 95 is the weakest bus of the IEEE 118-bus test system and shown in Figure 8. The highest improvement of total load compared to base case is provided by Case 2 (52.75% enhancement, 2.9639 p.u.). However, Cases 3 and 4 can increase margin to 2.6273 p.u. (35.41% enhancement) and 2.1511 p.u. (10.86% enhancement).

It can be observed that the voltage at the weakest bus of the IEEE 30-bus and 57-bus test systems is improved for all

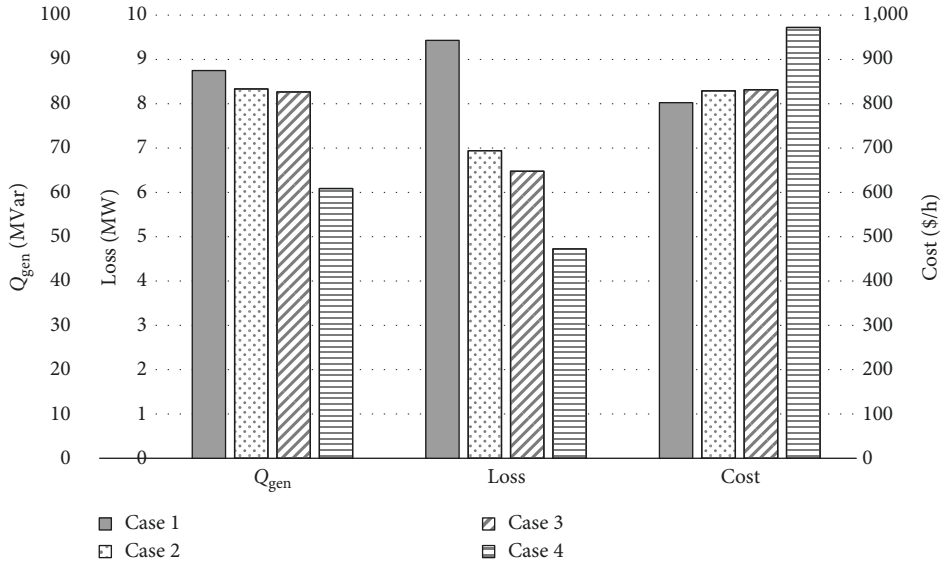

Figure 3: Variable comparisons for the IEEE 30-bus test system.

Table 2: System performance of the IEEE 57-bus test system.

	Objective functions			
	Case 1	Case 2	Case 3	Case 4
P_g (MW)	1,268.30	1,265.17	1,264.58	1,265.62
Q_g (MVar)	237.70	195.08	196.73	205.57
Loss (MW)	16.63	14.17	13.28	13.55
Cost ($/h)	41,828.39	42,122.71	42,078.60	44,054.27
Maximum FVSI	0.3408	0.2809	0.2411	0.3467
Maximum L_{mn}	0.3436	0.2830	0.2425	0.3494
Maximum LVSI	0.8731	0.8558	0.8572	0.8072
Sum FVSI	4.4305	2.8404	2.8147	4.7031
Sum L_{mn}	4.5054	2.8698	2.8463	4.7656
Sum LVSI	13.8230	12.7749	12.8361	12.5250
Maximum loadability (MW)	2,395.84	2,441.80	2,416.11	2,444.43

the proposed cases compared with base case. For the IEEE 30-bus test systems, the highest increase of voltage is Case 4. And the simulated result of Case 2 can provide the most improvement of voltage for the IEEE 57-bus test systems. Only Case 2 can increase the voltage level of weakest bus of the IEEE 118-bus test systems.

6.3. Line Outage Contingencies. Line outage contingencies generally change the system configuration, resulting in more stressful conditions. The power system may become less secure. Hence, the assessment of the contingency effect is important to maintain the system security. For this study, the maximum value of line stability indices is used to determine the contingency ranking. The line with highest value is identified as the most critical line and therefore selected to assess the effect of the contingency condition. The chosen buses for the IEEE 30-bus, 57-bus, and 118-bus test systems are line 30-27 (connecting buses 30 and 27), line 8-9, and line 38-65, respectively.

All proposed cases performed well in the line outage conditions. Table 4 shows the reactive power generation, power losses, generation cost, and maximum loadability. First, the reactive power generation is reduced for all the proposed cases compared with base case. For the IEEE 30-bus test system, Case 4 provides the best improvement with 59.58 MVar less by 35.23% compared with 91.98 MVar obtained in Case 1 (base case). Reactive power generation of Cases 2 and 3 are 83.99 MVar and 82.90 MVar, respectively. Q_g of the IEEE 57-bus test system is 282.05 MVar for Case 1. However, in Cases 2, 3, and 4, Q_g can reduce to 262.91 MVar, 265.46 MVar, and 276.98 MVar, respectively. For the IEEE 118-bus test system, the most reduction of reactive power generation is provided by Case 2 with 251.41 MVar less by 16.81% compared with 302.22 MVar obtained in Case 1. The results of Cases 3 and 4 are 295.41 MVar (2.25% reduction) and 258.13 MVar (14.59% reduction) of Q_g.

Second, the transmission losses for line outage contingencies were assessed. Compared to the previous section, the transmission losses are increased due to the line outage contingencies. The loss improvement of the proposed control approaches is greater than the base case. For the IEEE 30-bus test system, Case 4 gives the best result with 47.15% reduction compared with base case. The reduction levels of Cases 2 and 3 are 26.39% and 31.88%, respectively. Transmission loss of the IEEE 57-bus test system is alleviated for all proposed cases. Case 4 achieves the best reduction with 17.63 MW (17.94% reduction) of loss. However, the losses of Cases 2 and 3 are 20.80 MW and 18.97 MW, respectively. Loss of the IEEE 118-bus test system is significantly improved in Case 2 with a reduction of about 41.27% (49.65 MW). Cases 3 and 4 can reduce to 71.91 MW and 68.57 MW, respectively, corresponding to the 14.94% and 18.90% reduction.

Third, the maximum loadability enhancement for the selected case studies is expressed. The percentage increase in the maximum loadability is compared to the postcontingency data. All the proposed cases significantly increased the margin compared to the base case. For the IEEE 30-bus test system, the simulation results indicated substantial improvement in

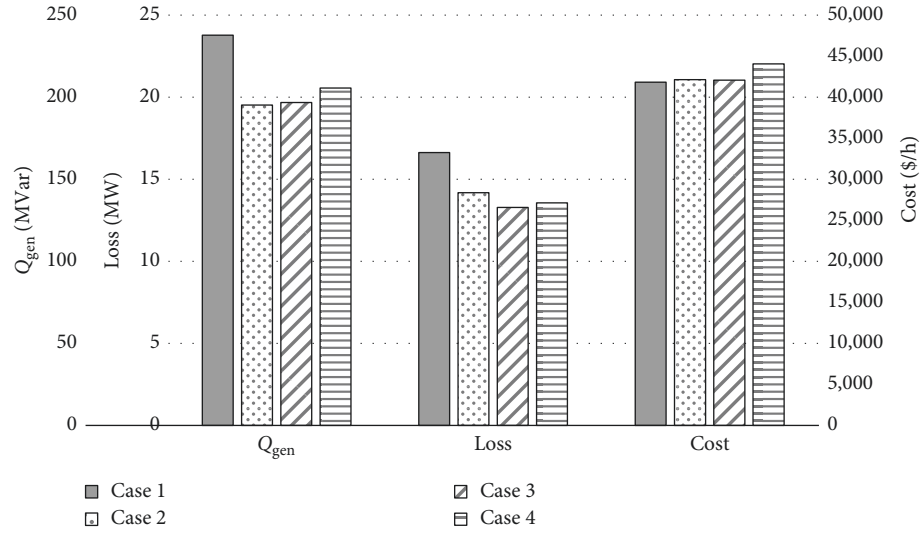

Figure 4: Variable comparisons for the IEEE 57-bus test system.

Table 3: System performance of the IEEE 118-bus test system.

	Objective functions			
	Case 1	Case 2	Case 3	Case 4
P_g (MW)	4,317.40	4,312.46	4,317.68	4,310.57
Q_g (MVar)	249.98	167.77	232.22	183.09
Loss (MW)	67.88	58.94	64.35	65.16
Cost ($/h)	144,225.06	150,129.63	155,450.07	149,882.80
Maximum FVSI	0.3913	0.2600	0.2750	0.3068
Maximum L_{mn}	0.3980	0.2670	0.2861	0.3514
Maximum LVSI	1.0000	0.9878	0.9834	0.9982
Sum FVSI	11.3469	10.6039	8.7766	9.2529
Sum L_{mn}	11.5817	10.8010	8.9422	9.4803
Sum LVSI	58.6067	54.7991	54.6839	58.3085
Maximum loadability (MW)	20,906.84	23,101.25	21,964.12	21,139.85

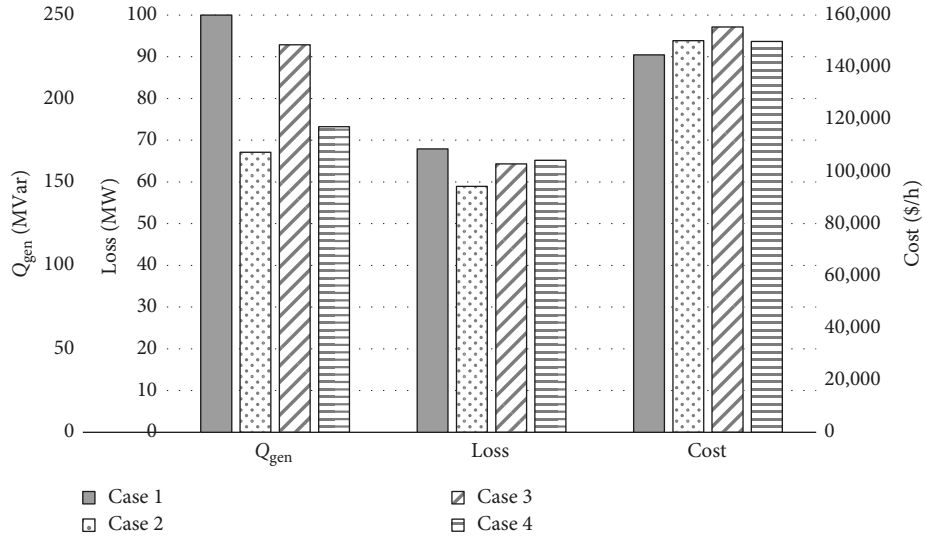

Figure 5: Variable comparisons for the IEEE 118-bus test system.

the voltage stability margin for all the proposed control approaches. The maximum loadability of the system is enhanced to 608.28 MW for Case 2, 593.71 MW for Case 3, and 611.49 MW for Case 4, whereas the base case provides 593.44 MW. For the IEEE 57-bus test system, all the proposed control approaches enhanced the voltage stability margin.

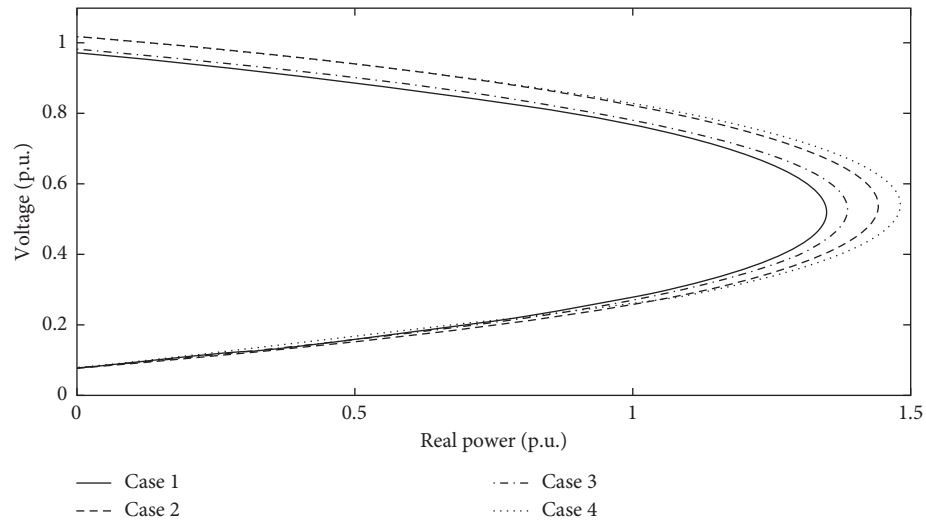

Figure 6: PV curves at the weakest bus of the IEEE 30-bus test system.

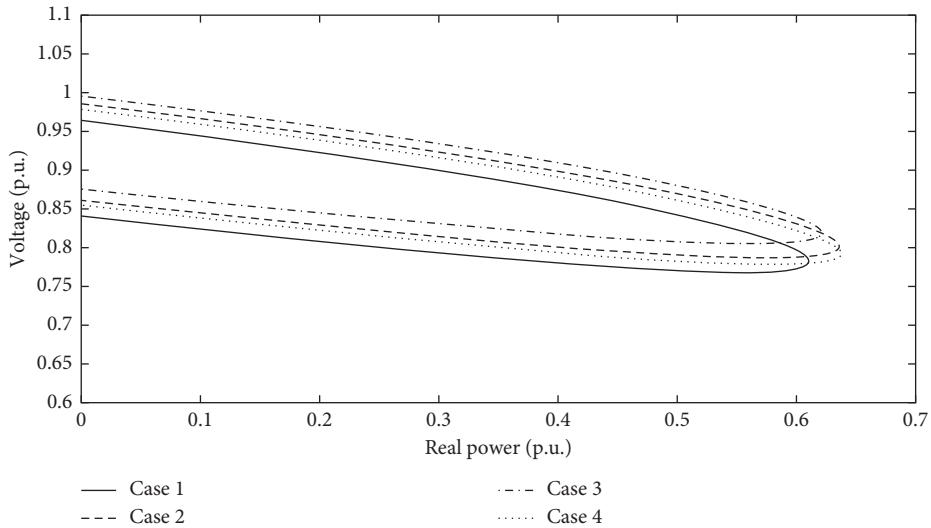

Figure 7: PV curves at the weakest bus of the IEEE 57-bus test system.

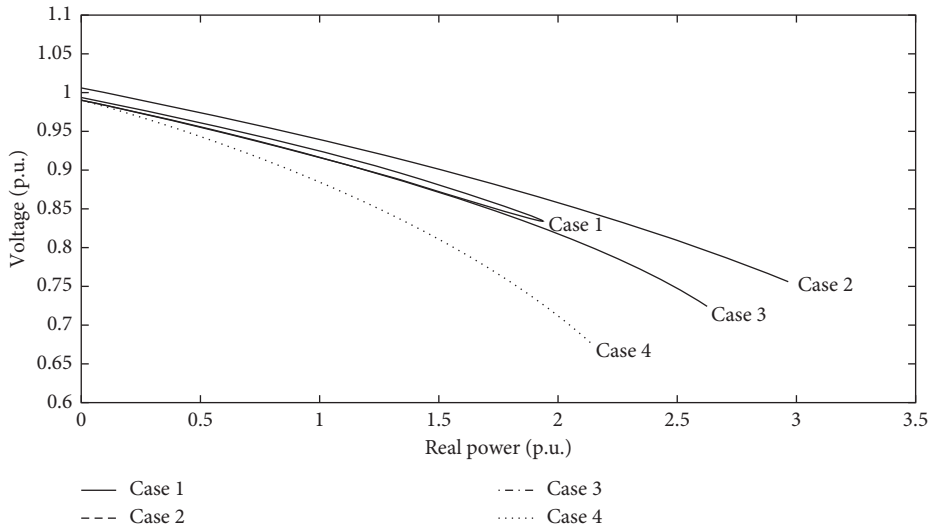

Figure 8: PV curves at the weakest bus of the IEEE 118-bus test system.

Table 4: System performance for line outage contingencies.

Test system	Variable	Objective functions			
		Case 1	Case 2	Case 3	Case 4
IEEE 30-bus test system	Q_g (MVar)	91.98	83.99	82.90	59.58
	Loss (MW)	9.86	7.26	6.72	5.21
	Maximum loadability (MW)	593.44	608.28	593.71	611.49
	Cost ($/h)	803.81	826.89	846.04	972.72
IEEE 57-bus test system	Q_g (MVar)	282.05	262.91	265.46	276.98
	Loss (MW)	21.48	20.80	18.97	17.63
	Maximum loadability (MW)	2,374.60	2,379.13	2,387.12	2,448.90
	Cost ($/h)	43,258.85	45,882.94	46,344.09	46,415.52
IEEE 118-bus test system	Q_g (MVar)	302.22	251.41	295.41	258.13
	Loss (MW)	84.54	49.65	71.91	68.57
	Maximum loadability (MW)	16,588.36	23,092.41	21,671.22	17,929.17
	Cost ($/h)	144,668.60	156,898.64	165,175.54	152,214.65

Based on the simulated results, the maximum loadability of the base case is 2,374.60 MW. Case 2 can increase loadability to 2,379.13 MW. Cases 3 and 4 also provide the greater level of loadability at 46,344.09 MW and 46,415.52 MW, respectively. Furthermore, for the IEEE 118-bus test system, Case 2 is able to raise the highest loadability with 39.21% increase from the base case. The loadability levels of Cases 3 and 4 are 21,671.22 MW (30.64% enhancement) and 17,929.17 MW (8.08% enhancement), respectively. As a result, the proposed control approaches are able to mitigate the voltage collapse, especially when the system is relieved from contingency conditions to a more secure level.

Fourth, the increase in the cost for all the proposed approaches is similar to the postcontingency cost, which is imposed for the security cost. The highest generation cost of the IEEE 30-bus test system is in Case 4 with 21.01% increase from base case. Cases 3 and 4 cost 2.87% and 5.25% higher than Case 1. For the IEEE 57-bus test system, costs of Cases 2, 3, and 4 are 6.07%, 7.13%, and 7.30% increase from the base case, respectively. The results of the IEEE 118-bus test system indicate that Case 3 imposes the highest cost with 14.18% greater than base case. Cases 2 and 4 give 8.45% and 5.22% increase in the generation cost.

Indeed, the incorporation of LVSI into objective function (Case 4) achieves the best reactive power generation, transmission loss, and maximum loadability for the IEEE 30-bus test system. Case 4 also provides the great results for the IEEE 57-bus test system. The use of FVSI summation as objective function (Case 2) is shown to be more efficient for the larger bus system as indicated in the IEEE 118-bus test system. Obviously, all proposed approaches demonstrate the effective improvement in both system stability and losses in the event of line outage contingencies. Therefore, all the proposed control approaches are potential countermeasures for relieving the stressful conditions.

7. Conclusions

In this paper, the voltage security-constrained optimal power flow (VSC-OPF) based on static line voltage stability indices is presented. The proposed control approaches are formulated into the conventional optimal power flow to enhance the static voltage stability margin and reduce the system losses. Minimization of the sums of fast voltage stability index (FVSI), line stability index (L_{mn}), and line voltage stability index (LVSI) is used to develop the objective functions. Lower values of the indices indicate higher levels of voltage stability improvement.

The performance and effectiveness of the proposed control approaches are investigated on the IEEE 30-bus, 57-bus, and 118-bus test systems. The analysis is carried out with different cases including minimization of the generation cost. The simulation results clearly indicate that all proposed control approaches increase the static voltage stability margin and minimize the system losses under normal and contingency conditions. For line outage contingencies, all the proposed control approaches significantly improved the static voltage stability margin and losses after contingencies. Therefore, the proposed control approaches can be considered efficient preventive control measures for contingency conditions, preventing voltage collapse. However, these approaches need to be judiciously chosen because the performance of the approaches will depend on the situation and size of the system.

All proposed control approaches are based on the simple concept that the complexity of the problem can be reduced. These approaches would be applicable for practical power system operation in today's competitive market. The multiobjective optimization problem approach that incorporates the static line voltage stability indices could be used in future studies on voltage stability improvement.

Data Availability

Research data used to support the findings of this study are available from the corresponding author upon request.

Conflicts of Interest

The authors declare that they have no conflicts of interest.

References

[1] B. Gao, G. K. Morison, P. Kundur et al., "Towards the development of a systematic approach for voltage stability

assessment of large-scale power systems," *IEEE Transactions on Power Systems*, vol. 11, no. 3, pp. 1314–1324, 1996.

[2] IEEE/PES Power System Stability Subcommittee, *Voltage Stability Assessment: Concepts, Practices and Tools, Special Publication*, vol. 11, no. 21–22, IEEE Power Engineering Society, Power System Stability Subcommittee Special Publication, Piscataway, NJ, USA, 2002.

[3] T. Nagao, K. Tanaka, and K. Takenaka, "Development of static and simulation programs for voltage stability studies of bulk power system," *IEEE transactions on power systems*, vol. 12, no. 1, pp. 273–281, 1997.

[4] P. Kundur, *Power System Stability and Control*, McGraw-Hill, New York, NY, USA, 2004.

[5] C. A. Canizares, A. C. Z. De Souza, and V. H. Quintana, "Comparison of performance indices for detection of proximity to voltage collapse," *IEEE Transactions on Power Systems*, vol. 11, no. 3, pp. 1441–1450, 1996.

[6] R. Wang and R. H. Lasseter, "Re-dispatching generation to increase power system security margin and support low voltage bus," *IEEE Transactions on Power Systems*, vol. 15, no. 2, pp. 496–501, 2000.

[7] A. Rabiee, N. Amjady, and H. Shayanfar, "Reactive power market development considering power system security," *Electrical Engineering*, vol. 92, no. 4-5, pp. 151–164, 2010.

[8] B. D. Thukaram and K. Parthasarathy, "Optimal reactive power dispatch algorithm for voltage stability improvement," *International Journal of Electrical Power and Energy Systems*, vol. 18, no. 7, pp. 461–468, 1996.

[9] D. Devaraj, "Improved genetic algorithm for multi-objective reactive power dispatch problem," *European Transactions on Electrical Power*, vol. 17, no. 6, pp. 569–581, 2007.

[10] D. Devaraj and J. P. Roselyn, "Genetic algorithm based reactive power dispatch for voltage stability improvement," *International Journal of Electrical Power and Energy Systems*, vol. 32, no. 10, pp. 1151–1156, 2010.

[11] M. S. Kumari and S. Maheswarapu, "Enhanced genetic algorithm based computation technique for multi-objective optimal power flow solution," *International Journal of Electrical Power and Energy Systems*, vol. 32, no. 6, pp. 736–742, 2010.

[12] T. Niknam, M. R. Narimani, J. Aghaei, and R. Azizipanah-Abarghooee, "Improved particle swarm optimisation for multi-objective optimal power flow considering the cost, loss, emission and voltage stability index," *IET Generation, Transmission and Distribution*, vol. 6, no. 6, pp. 515–527, 2012.

[13] S. Duman, U. Güvenç, Y. Sönmez, and N. Yörükeren, "Optimal power flow using gravitational search algorithm," *Energy Conversion and Management*, vol. 59, pp. 86–95, 2012.

[14] H. Xiong, H. Cheng, and H. Li, "Optimal reactive power flow incorporating static voltage stability based on multi-objective adaptive immune algorithm," *Energy Conversion and Management*, vol. 49, no. 5, pp. 1175–1181, 2008.

[15] C. Dai, W. Chen, Y. Zhu, and X. Zhang, "Reactive power dispatch considering voltage stability with seeker optimization algorithm," *Electric Power Systems Research*, vol. 79, no. 10, pp. 1462–1471, 2009.

[16] C. Roman and W. Rosehart, "Evenly distributed Pareto points in multi-objective optimal power flow," *IEEE Transactions on Power Systems*, vol. 21, no. 2, pp. 1011-1012, 2006.

[17] F. Capitanescu, M. Glavic, D. Ernst, and L. Wehenkel, "Interior-point based algorithms for the solution of optimal power flow problems," *Electric Power Systems Research*, vol. 77, no. 5-6, pp. 508–517, 2007.

[18] W. D. Rosehart, C. A. Caizares, and V. H. Quintana, "Effect of detailed power system models in traditional and voltage-stability-constrained optimal power-flow problems," *IEEE Transactions on Power Systems*, vol. 18, no. 1, pp. 27–35, 2003.

[19] B. Venkatesh, R. Ranjan, and H. B. Gooi, "Optimal reconfiguration of radial distribution systems to maximize loadability," *IEEE Transactions on power systems*, vol. 19, no. 1, pp. 260–266, 2004.

[20] P. A. Jeyanthy and D. Devaraj, "Optimal reactive power dispatch for voltage stability enhancement using real coded genetic algorithm," *International Journal of Computer and Electrical Engineering*, vol. 2, no. 4, pp. 734–740, 2010.

[21] H. Song, B. Lee, S. H. Kwon, and V. Ajjarapu, "Reactive reserve-based contingency constrained optimal power flow (RCCOPF) for enhancement of voltage stability margins," *IEEE transactions on Power Systems*, vol. 18, no. 4, pp. 1538–1546, 2003.

[22] H. Huang, Y. Kong, and J. Zhang, "The analysis on the L-index based optimal power flow considering voltage stability constraints," *WSEAS Transactions on Systems*, vol. 7, pp. 1300–1309, 2008.

[23] S. Jeyadevi, S. Baskar, and M. W. Iruthayarajan, "Reactive power planning with voltage stability enhancement using covariance matrix adapted evolution strategy," *European Transactions on Electrical Power*, vol. 21, no. 3, pp. 1343–1360, 2011.

[24] H. Song, B. Lee, and Y.-H. Moon, "Reactive optimal power flow incorporating margin enhancement constraints with nonlinear interior point method," *IEE Proceedings-Generation, Transmission and Distribution*, vol. 152, no. 6, pp. 961–968, 2005.

[25] G. Y. Wu, C. Y. Chung, K. P. Wong, and C. W. Yu, "Voltage stability constrained optimal dispatch in deregulated power systems," *IET Generation, Transmission and Distribution*, vol. 1, no. 5, pp. 761–768, 2007.

[26] D. Luo, X. Cao, H. He, and T. Lu, "Fast approach for voltage stability constrained optimal power flow based on load impedance modulus margin," in *Proceedings of 2017 IEEE Industry Applications Society Annual Meeting*, pp. 1–12, IEEE, Cincinnati OH, USA, October 2017.

[27] C. Wang, B. Cui, Z. Wang, and C. Gu, "SDP-based optimal power flow with steady-state voltage stability constraints," *IEEE Transactions on Smart Grid*, 2018.

[28] A. A. Mohamed and B. Venkatesh, "Linearized voltage stability incorporation with line-wise optimal power flow," *International Journal of Electrical Power and Energy Systems*, vol. 108, pp. 232–239, 2019.

[29] T. Zabaiou, L.-A. Dessaint, and I. Kamwa, "Preventive control approach for voltage stability improvement using voltage stability constrained optimal power flow based on static line voltage stability indices," *IET Generation, Transmission and Distribution*, vol. 8, no. 5, pp. 924–934, 2014.

[30] M. Kumar and P. Renuga, "Application of UPFC for enhancement of voltage profile and minimization of losses using fast voltage stability index (FVSI)," *Archives of Electrical Engineering*, vol. 61, no. 2, pp. 239–250, 2012.

[31] L. Jebaraj, C. C. A. Rajan, and S. Sakthivel, "Incorporation of SSSC and SVC devices for real power and voltage stability limit enhancement through shuffled frog leaping algorithm under stressed conditions," *European Journal of Scientific Research*, vol. 79, no. 1, pp. 119–132, 2012.

[32] M. B. Wafaa and L.-A. Dessaint, "Multi-objective stochastic optimal power flow considering voltage stability and demand response with significant wind penetration," *IET Generation, Transmission and Distribution*, vol. 11, no. 14, pp. 3499–3509, 2017.

[33] S. Khunkitti, S. Premrudeepreechacharn, R. Chatthaworn et al., "A comparison of the effectiveness of voltage stability indices in an optimal power flow," *IEEJ Transactions on Electrical and Electronic Engineering*, vol. 14, no. 4, pp. 534–544, 2018.

[34] I. Musirin and T. A. Rahman, "Novel fast voltage stability index (FVSI) for voltage stability analysis in power transmission system," in *Proceedings of the Student Conference on Research and Development, SCOReD 2002*, pp. 265–268, IEEE, Alam, Malaysia, July 2002.

[35] M. Moghavvemi and G. B. Jasmon, "New method for indicating voltage stability condition in power system," in *Proceedings of theThird International Conference on Power Engineering*, vol. 1, pp. 223–227, Singapore, May 1997.

[36] N. S. Hang, T. Xu, Q. H. Liao, and Z. Q. Lu, "The analysis of abundance index of voltage stability based circuit theory," *Guangxi Electric Power*, vol. 2, p. 002, 2006.

[37] S. Khunkitti, A. Siritaratiwat, S. Premrudeepreechacharn, R. Chatthaworn, and N. Watson, "A hybrid DA-PSO optimization algorithm for multiobjective optimal power flow problems," *Energies*, vol. 11, no. 9, p. 2270, 2018.

[38] T. Niknam, M. r. Narimani, M. Jabbari, and A. R. Malekpour, "A modified shuffle frog leaping algorithm for multi-objective optimal power flow," *Energy*, vol. 36, no. 11, pp. 6420–6432, 2011.

[39] S. Mirjalili, "Dragonfly algorithm: a new meta-heuristic optimization technique for solving single-objective, discrete, and multi-objective problems," *Neural Computing and Applications*, vol. 27, no. 4, pp. 1053–1073, 2016.

[40] R. Eberhart and J. Kennedy, "A new optimizer using particle swarm theory," in *Proceedings of the Sixth International Symposium on Micro Machine and Human Science, MHS'95*, pp. 39–43, IEEE, Nagoya, Japan, October 1995.

[41] The University of Washington Electrical Engineering, "Power system test case archive, the IEEE 30-bus test system data," October 2017, https://www2.ee.washington.edu/research/pstca/pf30/pg_tca30bus.htm.

[42] The University of Washington Electrical Engineering, "Power system test case archive, the IEEE 57-bus test system data," October 2017, https://www2.ee.washington.edu/research/pstca/pf57/pg_tca57bus.htm.

[43] The Electrical and Computer Engineering Department, Illinois Institute of Technology, "Data power system test case archive, the IEEE 118-bus test system data," October 2017, http://motor.ece.iit.edu/data/JEAS_IEEE118.doc.

[44] *Matlab Optimization Toolbox, (R2011a)*, The MathWorks Inc., Natick, MA, USA, 2011.

[45] R. D. Zimmerman, C. Murillo-Sánchez, and R. J. Thomas, "MATPOWER: steady-state operations, planning and analysis tools for power systems research and education," *IEEE Transactions on Power Systems*, vol. 26, no. 1, pp. 12–19, 2011.